American Journal of Pathology, Vol. 163, No. 5, November 2003

Animal Model

Progression to Malignancy in the Polyoma Middle T Oncoprotein Mouse Breast Cancer Model Provides a Reliable Model for Human Diseases

Elaine Y. Lin,* Joan G. Jones,† Ping Li,* Liyin Zhu,* Kathleen D. Whitney,† William J. Muller,‡ and Jeffrey W. Pollard*

From the Center for Study of Reproductive Biology and Women's Health and the Departments of Developmental and Molecular Biology and Obstetrics and Gynecology and Women's Health, and the Department of Pathology,† Albert Einstein College of Medicine, Bronx, New York; and the Department of Medicine and Biochemistry,‡ McGill University, Montreal, Quebec, Canada*

Animal models are powerful tools to analyze the mechanism of the induction of human breast cancer. Here we report a detailed analysis of mammary tumor progression in one mouse model of breast cancer caused by expression of the polyoma middle T oncoprotein (PyMT) in the mammary epithelium, and its comparison to human breast tumors. In PyMT mice, four distinctly identifiable stages of tumor progression from premalignant to malignant stages occur in a single primary tumor focus and this malignant transition is followed by a high frequency of distant metastasis. These stages are comparable to human breast diseases classified as benign or *in situ* proliferative lesions to invasive carcinomas. In addition to the morphological similarities with human breast cancer, the expression of biomarkers in PyMT-induced tumors is also consistent with those associated with poor outcome in humans. These include a loss of estrogen and progesterone receptors as well as integrin-β1 expression and the persistent expression of ErbB2/Neu and cyclinD1 in PyMT-induced tumors as they progress to the malignant stage. An increased leukocytic infiltration was also closely associated with the malignant transition. This study demonstrates that the PyMT mouse model is an excellent one to understand the biology of tumor progression in humans. *(Am J Pathol 2003, 163:2113–2126)*

Breast cancer has the highest incidence among women in the Western world affecting up to 10% of women in the future and therefore is among today's most pressing health problems.[1] Despite improvements in diagnosis, treatment, and longevity, the effect on mortality has been modest.[1] A lack of understanding about the natural history of the disease is a major contributory factor to this limitation.[2] On a molecular level it is still unclear which of the changes in breast tumors are likely to lead to invasion and metastasis. The application of transgenic technology in mice to study the progression of mammary cancer has proven extremely powerful to understand important principles of tumorigenesis and evaluating response to therapy.[3–6] However, few of these models reflect the complexity of human breast cancers, especially their progression to metastasis.

Previously we have reported that we chose one of the breast cancer transgenic mouse models whose oncogenesis is induced by expression of the polyoma virus middle T oncoprotein (PyMT mice) to study the effect of the mononuclear phagocyte growth factor, colony-stimulating factor-1 (CSF-1) in mammary tumor progression.[7] In this model, the expression of the oncoprotein, polyoma middle T antigen (PyMT), is under the control of mouse mammary tumor virus LTR (MMTV LTR) and is therefore restricted to the mammary epithelium. Mammary hyperplasia can be detected in this model as early as 4 weeks[7,8] and most importantly, a large percentage of mice developed carcinoma at ~14 weeks and this correlated with the appearance of pulmonary metastases.[7] PyMT, a membrane-attached protein, is encoded by the small DNA polyoma virus. PyMT is not expressed in human breast tumor cells, however, it acts as a potent

Supported by the Analytical Imaging Facility and Histotechnology and Comparative Pathology Facility at Albert Einstein College of Medicine; the Albert Einstein College Comprehensive Cancer Center (P30-CA13330), and the National Institutes of Health (RO1CA094173).

JWP is the Sheldon and Betty E. Feinberg Senior Faculty Scholar in Cancer Research and EYL was a recipient of National Research Service Award 5-T32-AG00194.

Accepted for publication July 28, 2003.

Address reprint requests to Jeffrey W. Pollard, 607 Chanin Building, Albert Einstein College of Medicine, 1300 Morris Park Ave., Bronx, NY 10461. E-mail: pollard@aecom.yu.edu.

oncogene because its product binds to and co-opts several signal transduction pathways, including those of the *Src* family and the *ras* and PI3 kinase pathways, which are altered in human breast cancers.[9] In addition, in PyMT mice mammary glands, the expression of PyMT is found to be associated with an increased *c-myc* level,[8,10,11] a gene that is located in one of the three amplified chromosomal regions found in human primary breast cancers.[12]

In the present study to determine how relevant this PyMT model is for human breast cancer, we performed a detailed histological analysis and showed many similarities to the histology of human tumors. We also analyzed a series of biomarkers associated with poor prognosis in human breast cancers. Remarkably in the PyMT model, loss of estrogen and progesterone receptors (ERs and PRs) and overexpression of ErbB2/Neu and cyclin D1 are observed, that is recapitulated in a manner similar to that observed in human breast cancer with poor prognosis.[12–15] Moreover, there was altered expression of integrin-β, the molecule that plays an important role in regulating cell proliferation, differentiation, and apoptosis of normal mammary epithelium,[16] in these tumors during progression to malignancy. These studies indicate that the PyMT model recapitulates many processes found in human breast cancer progression not only morphologically but also in the pattern of expression of biomarkers associated with poor prognosis. Therefore, this mouse model of mammary carcinogenesis represents a powerful one to study the causal events associated with tumor progression to malignancy and metastasis.

Materials and Methods

Mice and Histology

All procedures involving mice were conducted in accordance with the National Institutes of Health regulations concerning the use and care of experimental animals. The study of mice was approved by the Albert Einstein College of Medicine animal use committee. Male PyMT mice on a C3H/B6 $\times$ FVB-C3H/B6 background were randomly bred with C3H/B6 females lacking the PyMT transgene to obtain female mice heterozygous for the PyMT transgene. All of the mice analyzed in this study were heterozygous for the PyMT transgene.

Right abdominal mammary glands were used for whole mount preparation as described previously.[17] Mammary glands were fixed in 10% formalin at 4°C overnight and then transferred to cold 70% ethanol. Tissues were paraffin-embedded, sectioned, and stained with hematoxylin and eosin (H&E).

Immunohistochemistry (IHC)

To identify cells expressing ER-α, PR, Erb2/Neu, and integrin-β1, formalin-fixed mammary gland sections were immunostained using rabbit polyclonal antibodies raised against the carboxyl terminus of the mouse ER-α, the human PR, the human Neu gp185, and the extracellular domain of human integrin-β1 (sc-542, sc-538, sc-284, and sc-8978 respectively; Santa Cruz Biotechnology Inc., Santa Cruz, CA). To identify cells expressing cyclin D1, sections were stained with a mouse monoclonal antibody against cyclin D1 (DCS-6; NeoMarkers, Freemont, CA) as described.[18] For IHC of α-smooth muscle actin (SMA) and laminin α1, mouse monoclonal anti-SMA (A-2547; Sigma Chemical Co., St. Louis, MO) and an affinity-purified goat polyclonal antibody raised against mouse laminin α1 (sc-6017, Santa Cruz Biotechnology) were used. To eliminate nonspecific interactions of secondary antibodies, tissues were incubated with 10% normal serum from the same host that had been used to generate the secondary antibodies, at 25°C for 1 hour and then with the primary antibodies at 4°C overnight (anti-ER-α, 1 μg/ml; anti-PR, 0.7 μg/ml; anti-Neu, 0.5 μg/ml; anti-cyclin D1, 1 μg/ml; laminin α1 and integrin-β1, 2 μg/ml; and SMA, 1:400). Heat treatment of tissue sections in sodium citrate buffer was performed for the staining of the anti-ER-α antibody following the procedure provided by Santa Cruz Biotechnology Inc. Specific reactivity was detected using a peroxidase-based detection kit (Vector Laboratories, Burlingame, CA) as described.[19] As a negative control of the staining, adjacent sections were incubated with primary antibodies blocked with specific peptides (5 μg/ml) for ER-α, PR, or Neu (sc-542 P, sc-538 P, or sc-284 P, respectively; Santa Cruz Biotechnology, Inc.) at 4°C overnight.

Western Blotting Analysis

For normal tissues used as a control, whole mammary glands or uterus were removed from mice at the ages indicated and frozen immediately in dry ice until use. The hormonal treatment of mice was described previously.[18] To prepare primary tumors at an early age before the tumor was visible, part of fourth mammary gland, from the nipple to the mid line between nipple and subiliac lymph node, was collected. For visible tumors, the tumor was carefully dissected away from the surrounding tissues. The tissue was homogenized and then sonicated at 4°C in RIPA buffer consisting of 1% Nonidet P-40, 1% sodium dodecyl sulfate, 0.5% sodium dexocholate, protease inhibitor cocktail (Sigma Chemical Co.), and phosphate-buffered saline buffer (pH 7) for 5 and 2 minutes, respectively. Western gel preparation and immunoblotting were performed following standard procedures.[20]

Results

The Morphology of PyMT Tumors during Progression Is Comparable to Human Breast Cancers

Mammary tumors occur in every PyMT mouse by 4 weeks of age.[8] As seen in mammary whole-mount preparations, a single focus, or occasionally a few apposed foci, develops first around the main collecting duct just beneath the nipple (Figure 1A, PT). This is followed in older mice by multiple

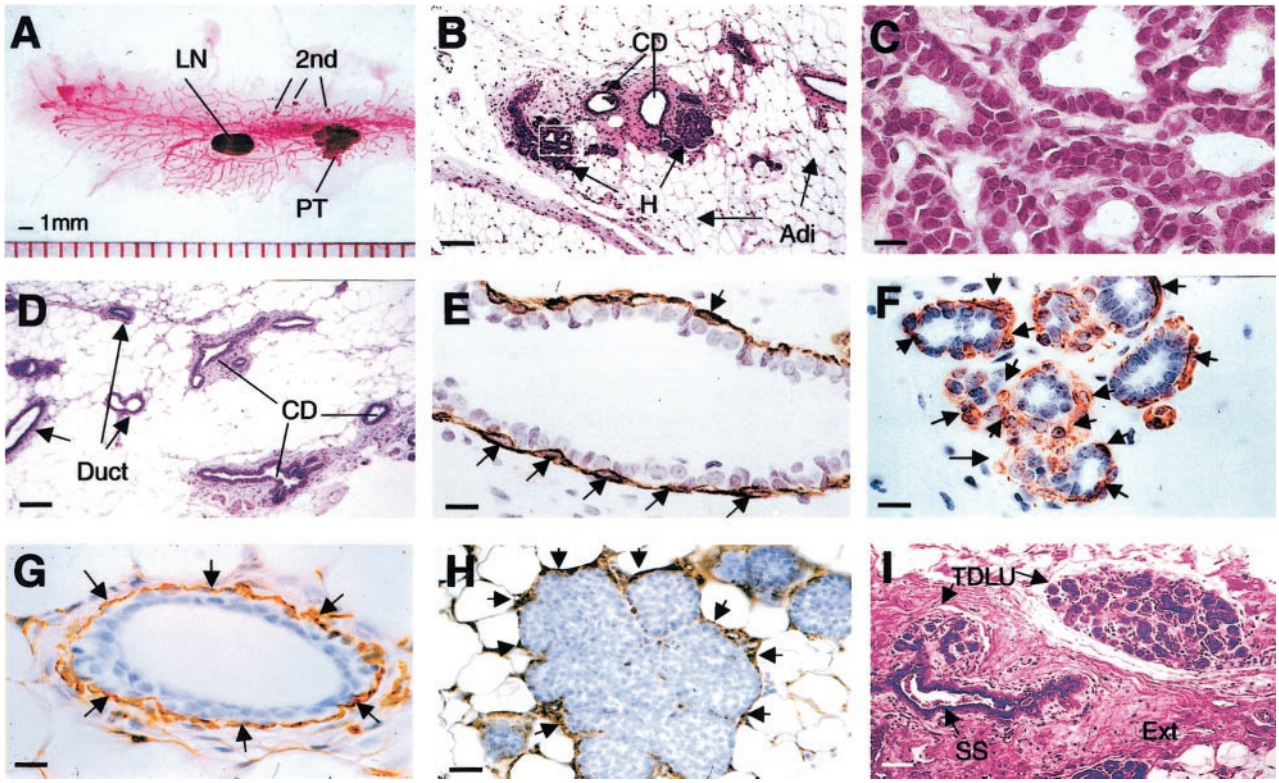

Figure 1. Early premalignant tumor in PyMT mice is comparable to human normal breast. **A:** Carmine red-stained whole-mount preparation of mammary gland from a PyMT mouse at 8 weeks of age. PT, primary tumor; second, foci growing on the distant ducts; LN, lymph note. **B:** H&E staining of a mammary gland prepared from a PyMT mouse at 4 weeks of age. CD, main milk-collecting ducts; H, the hyperplastic lesion; Adi, adipose cells. The **inset** in **B** is shown in **C**. **D:** H&E staining of a mammary gland section from a normal mouse at 4 weeks of age. **E** and **F:** IHC of SMA in a normal mouse mammary duct (**E**) and a hyperplastic lesion (**F**). **Arrows** point to the positively stained myoepithelial cells. **G** and **H:** IHC of laminin α1 in a normal mouse mammary duct (**G**) and a hyperplastic lesion (**H**). **Arrows** point to some of the positively stained areas. **I:** H&E staining of a normal human breast. TDLU, terminal duct lobular unit; SS, subsegmental duct; Ext, extracellular fibers. Note that SS leads to TDLU. The earliest change in the mouse lesion is an alteration in the mammary architecture that produces a lobular-alveolar structure that looks similar to the normal TDLU of the human. Scale bars: 100 μm (**B**, **D**, **I**); 25 μm (**H**); 10 μm (**C**, **E**, **F**, **G**). Original magnifications: $\times$100 (**B**, **D**, **I**); $\times$1000 (**C**, **E**, **F**, **G**); $\times$400 (**H**).

small nodules forming along the more distal ducts (Figure 1A, second). Distinct histopathological changes representing morphological events of tumor progression from benign to malignant are observed in this first tumor focus, designated as the primary tumor.[7] We have developed a four-stage classification scheme that includes hyperplasia, adenoma/mammary intraepithelial neoplasia (MIN), and early and late carcinoma. These stages are in accordance with but refine for this PyMT model, the recommendations for the classification of mouse mammary tumor pathology panel.[21]

Premalignant Lesions

Hyperplasia, the Earliest Change in the PyMT Mammary Gland

Fifty to 60% of the PyMT mice examined at 4 to 6 weeks of age have primary tumors developed to the hyperplastic stage.[7] The hyperplastic lesion typically consists of a cluster(s) of densely packed lobules formed on the duct that connects to the main milk-collecting duct (Figure 1B) and in some cases, the hyperplastic acinus is filled or bridged with epithelial cells (Figure 1H). Cytologically, the cells in these proliferative lesions are bland, with only a slight increase in nuclear/cytoplasmic ratio in comparison to normal ductal cells (Figure 1C). Similar to normal ducts, a single layer of luminal epithelial cells surrounds a central lumen and sits atop a layer of myoepithelial cells, as shown by the staining of a myoepithelial marker, SMA [Figure 1, E (a normal duct) and F (hyperplasia)]. However, compared to the normal duct, in which myoepithelial cells often have flat cell bodies and occur with a relative equal spacing (Figure 1E, arrows), the myoepithelial cells in the hyperplastic lesion appear to have more rounded cell bodies and are distributed unevenly around tumor acini (Figure 1F, arrows). Both the morphologically normal ducts and the hyperplastic acini in the same mammary gland (Figure 1G) are surrounded by a well-developed basement membrane and connective tissue as assayed by laminin-α1 staining (Figure 1H, arrows). Although the cellular morphology of the hyperplastic lesion is similar to a normal duct, the architecture of the lesion, with a terminal duct entering a cluster of lobules, is not seen in the normal virgin mouse mammary gland, in which only ducts are found (Figure 1D).[22] Such a lobular-like structure, however, is similar to the lobular development found in the mouse mammary glands of early to mid-pregnant mice[22] and also appear similar in structure to the terminal duct lobular unit in a normal adult human breast (Figure 1I).[23] One marked difference be-

tween the mouse mammary gland and human breast tissue is that the mouse tumor and ducts are surrounded by a thin fibroblastic stroma adjacent to the adipocytes that form the majority of the gland and which are often very close to the epithelial structures (Figure 1B). In contrast, in humans, the lobules have extensive extracellular connective tissue stroma (Figure 1I, Ext), therefore the adipocytes are less proximal to the ductal epithelium.

Adenoma/MIN, an Advanced Premalignant Lesion

The term adenoma has previously been given to the primary tumors that occur in the majority of PyMT mice at 8 to 9 weeks of age.[7] In this model, adenoma describes a more florid epithelial proliferation still confined by a basement membrane, with minimal cytological atypia and with no evidence of invasion or metastasis. In the context of the consensus terminology article on genetically engineered mice from the Annapolis panel of pathologists,[21] this lesion has features of both an adenoma and MIN. As a mass, it qualifies as an adenoma, but in the Annapolis terminology, adenomas do not progress to malignancy whereas in the PyMT model these always appear to become malignant (see below). MIN lesions, on the other hand, are considered premalignant, but are not mass-producing. In this stage of our model, the cellular proliferation fills and expands the closely packed acini and ducts, markedly increasing the size of the primary tumor (Figure 2A). The acini are usually completely filled by solid sheets of relatively uniform cells, with round to oval nuclei (Figure 2B). The tumor acini at this stage are surrounded by a single layer of myoepithelial cells as determined by SMA immunostaining, although it is incomplete in many areas (Figure 2C). Similar to the normal mammary ducts in the mammary gland (Figure 2D), most of the tumor acini appear to have an intact basement membrane as assessed by laminin-α1 immunostaining (Figure 2E). There is no evidence of necrosis. Thus a more accurate terminology for this premalignant stage might be adenoma/MIN.

Although tumors at the hyperplastic stage have very few leukocytes in the surrounding stroma, some adenoma/MIN lesions do contain foci of leukocytic infiltration in the vicinity of the tumor (average one/primary tumor section) [Figure 2, A (arrow) and F (in higher magnification)]. These infiltrates are composed of cells with the morphology of macrophages, fibroblasts, and neutrophils. An increased vascularity is also observed at these sites (Figure 2F). The tumor acini adjacent to these infiltration sites appear to have lost the basement membrane as assessed by laminin-α1 staining (Figure 2G, open arrow), compared to the adjacent acini that are well surrounded by the laminin-positive basement membrane (Figure 2G, arrows).

The adenoma/MIN found in PyMT mammary glands is morphologically similar to florid ductal epithelial breast hyperplasia in humans (DHF) (Figure 2; H to I).[24] Although the patterns in the human are heterogeneous, in some, the pattern is that of solid sheets of cells filling the terminal duct lobular unit (Figure 2H) surrounded by a well-formed basement membrane and connective tissue. As in the adenoma/MIN of the PyMT mice, the cells are relatively uniform (Figure 2I). Infiltration of leukocytes around the filled acinus is observed in some of these lesions (Figure 2H, arrows).

Malignant Lesions

Early Carcinoma, the Initial Stage of Malignant Transition

The defining feature of the early carcinoma stage compared with the adenoma/MIN in the mouse is the presence of greater cytological atypia and the identification of early stromal invasion. Within the same lesion, features of both adenoma/MIN and early carcinoma are usually present. The increased cytological atypia is a distinct morphological change typically found in the center of the primary tumor (Figure 3A, framed area is the center of the tumor that is shown in Figure 3B at higher magnification). In these areas of transition to malignancy, the tumor cells now appear pleomorphic, showing a moderate variation in nuclear morphology, size, and shape (Figure 3B). In addition to increased nuclear pleomorphism, the outline of individual tumor acini in these transition areas becomes unclear. The staining of basement membrane marker laminin-α1 in this area is often negative (Figure 3C, open arrows) or scattered in a random pattern that no longer resembles a basement membrane (Figure 3D, arrows). There is also a high density of leukocytic infiltration surrounding the tumor acini (Figure 3E, open arrows). The majority of infiltrating cells are mononuclear with macrophage morphology (Figure 3F) but a few granulocytes can also be seen (Figure 3F, long arrows). An increased vessel density is found in the vicinity of the tumor adjacent to the areas with dense leukocytic infiltration (Figure 3F, green arrows). The majority of the ducts in the mammary glands that carry these early carcinomas are still morphologically normal, except for focal areas in which there is mild ductal epithelial hyperplasia with a small increase in the number of cell layers (data not shown).

This early malignant transition occurs in PyMT mice between 8 to 12 weeks of age. PyMT tumors classified at this stage are morphologically similar to human ductal carcinoma *in situ* with early stromal invasion (Figure 3; G to I).[24] Similar to the mouse counterpart, this human lesion consists of distended acinar structures with focal stromal invasion (Figure 3G, arrows). The cytological atypia in the PyMT mice is analogous to the intermediate to high-grade human ductal carcinoma *in situ* (Figure 3H). High density of leukocytic infiltration is often observed in the human tumor (Figure 3I, arrows).

Late Carcinoma, Advanced Invasive Carcinoma

By 10 weeks of age, the primary tumors in ~50% of PyMT mice examined have progressed to the advanced carcinoma stage, termed late carcinoma. At this stage the tumor is composed of solid sheets of epithelial cells with little or no remaining acinar structures visible (Figure

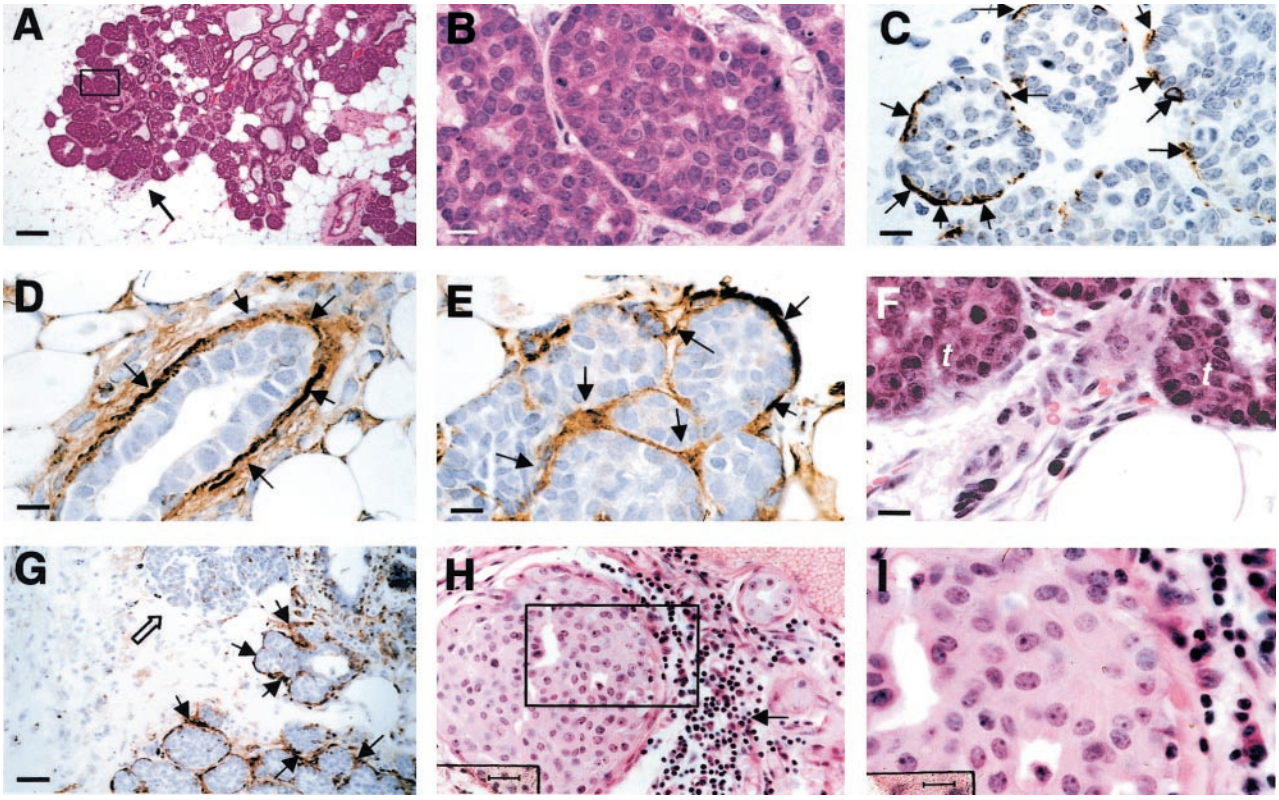

Figure 2. Adenoma/MIN in PyMT mice is comparable to human ductal hyperplasia, florid (DHF). **A** and **B:** H&E staining of mammary gland sections from a PyMT mouse at 8 weeks of age. **A:** A primary mammary lesion at adenoma/MIN stage. **Arrow** points to an infiltration site of leukocytes showing in **F** at higher magnification. The **inset** in **A** is shown in **B**. **C:** IHC of SMA in a primary tumor at adenoma/MIN stage. **Arrows** point to the positively stained myoepithelial cells surrounding the lesion. **D** and **E:** IHC of laminin α1 in a normal mammary duct (**D**) and an adenoma/MIN lesion (**E**). **Arrows** point to positively stained areas. **F:** An enlarged image of the leukocytic infiltration site from **A**. t, tumor. **G:** IHC of laminin α1 in an adenoma/MIN-stage lesion consisting of a leukocytic infiltration site. Note that in contrast to the adjacent acini, which are surrounded by laminin α1-positive basement membrane (**arrows**), the acina adjacent to the leukocytic infiltration site has no positive staining of laminin α (**open arrow**). **H:** H&E staining of a human proliferative breast lesion, DHF. The **arrow** points to infiltrated leukocytes adjacent to the lesion. The **inset** in **H** is shown in **I**. Scale bars: 100 μm (**A**); 10 (**B–F**, **I**); 40 μm (**G**); 25 (**H**). Original magnifications: ×100 (**A**); ×1000 (**B**, **C**, **D**, **E**, **F, I**); ×250 (**G**); ×400 (**H**).

4A). The malignant cells in the tumor have marked variation in cellular and nuclear size and shape with vesicular nuclei and prominent nucleoli (Figure 4B). A significant increase in mitotic index is observed. Negative staining of laminin-α1 is found in the tumor although still found on the adjacent ducts (Figure 4C, arrow). At this late carcinoma stage, multiple tumor nodules as well as ductal hyperplasia are found throughout the mammary gland (data not shown).

PyMT tumors at this late carcinoma stage have many characteristics that are similar to a human breast cancer classified as poorly differentiated invasive ductal carcinoma.[24] These lesions also consist of solid sheets of malignant cells (Figure 4D) with marked variation in cell shape, size, and nuclear morphology (Figure 4E). The invasive tumor cells are associated with a reactive stroma, which consists of fibroblasts and leukocytes in a background of newly laid down eosinophilic matrix (Figure 4F, arrows).

Multiple Foci Develop in the Mammary Glands of PyMT Mice

In addition to the tumor focus formed on the main milk-collecting duct, multiple foci are also formed on the distant ducts in older mice. These later-appearing nodules appear to develop in a random manner. They are often seen in multiple locations but occasionally develop contiguously along a branch of duct in the mammary gland. Approximately 70% of PyMT mice examined at 6 weeks of age had developed a few such foci (Figure 1); however, at 14 weeks of age, all mice had developed secondary tumors in the mammary glands that eventually affect the entire gland. In general, these secondary growths are one or two stages behind the primary tumors in the same mammary gland but they eventually develop to invasive carcinoma and fuse with the primary nodule to form one solid tumor.

Loss of ER and PR in PyMT Mice Correlates with Tumor Progression to Malignancy

Estrogen- and progesterone-receptor (ER and PR) expression is routinely used to determine the prognosis of human breast cancers with loss of expression being associated with poor prognosis.[13] To further examine the relevance of the PyMT model for studies on human breast cancer, the expression of ER-α and PR in the primary tumors of PyMT mice was examined using immunohisto-

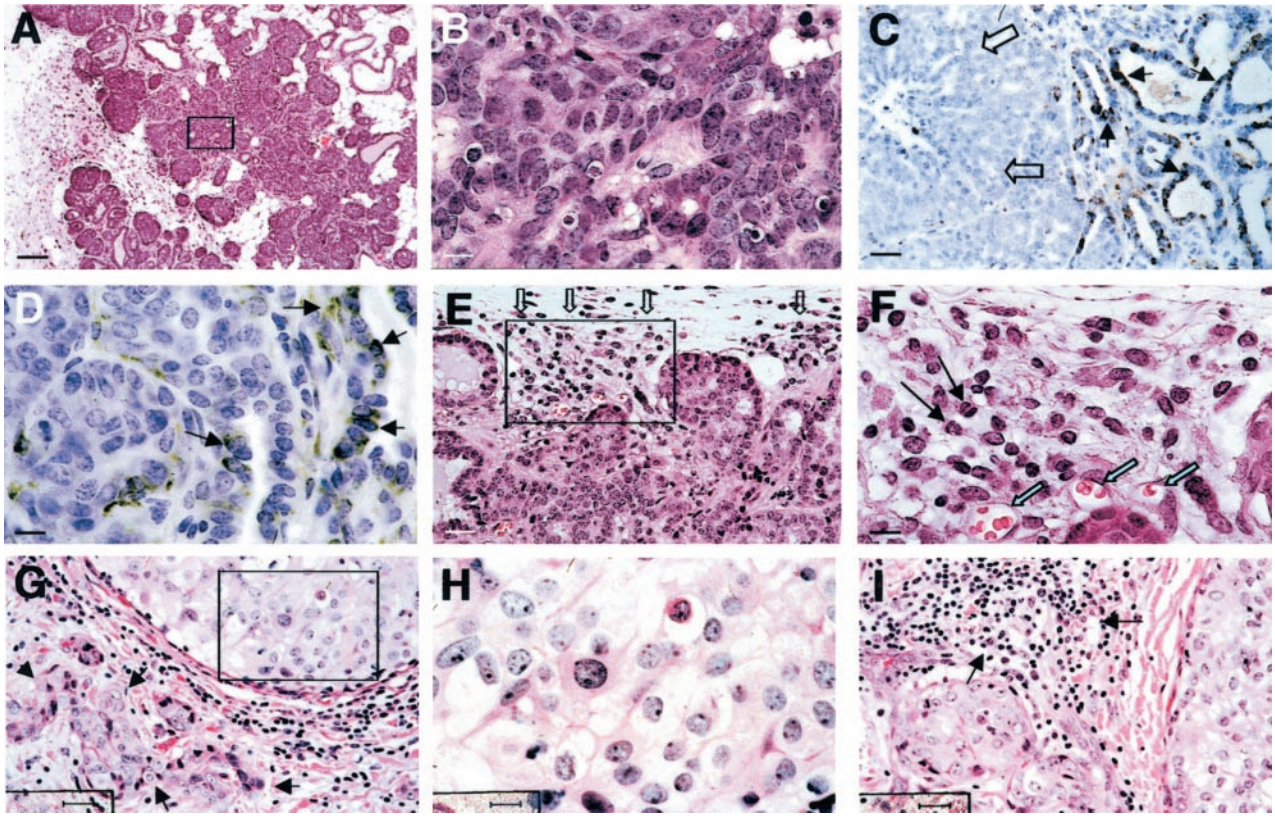

Figure 3. Early carcinoma in PyMT mice is comparable to human ductal carcinoma *in situ* with early invasion (DCIS+EI). **A:** H&E staining of mammary glands from a PyMT mouse at 9 weeks of age. The **inset** of **A** is shown in **B**. **C** and **D:** IHC of laminin α1 in a PyMT mammary tumor at the early carcinoma stage. Note that in **C**, the positive staining of laminin α1 is located in the periphery (**arrows**) but not in the center the lesion (**open arrows**). **D:** A scattered staining of laminin α1 in the center of a tumor at the early carcinoma stage. **E:** H&E staining of a early carcinoma showing high density of leukocytic infiltration at the vicinity of the lesion. **Open arrows** point to the leukocytes. The **inset** in **E** is shown in **F**. **Long arrows** point to the granulocytes and **open green arrows** point to blood vessels. **G:** H&E staining of human proliferative lesion, DCIS+EI. **Arrows** point to the microinvasions in the tumor stroma. The **inset** of **G** is shown in **H**. Note the nuclear pleomorphism in the area. **I:** H&E staining of human DCIS+EI showing high density of leukocytic infiltration (**arrows**). Scale bars: 100 μm (**A**); 10 μm (**B**, **D**, **F**, **H**); 25 μm (**C**, **E**, **G**, **I**). Original magnifications: × 100 (**A**); ×1000 (**B**, **D**, **F**, **H**); ×400 (**C**, **E**, **G**, **I**).

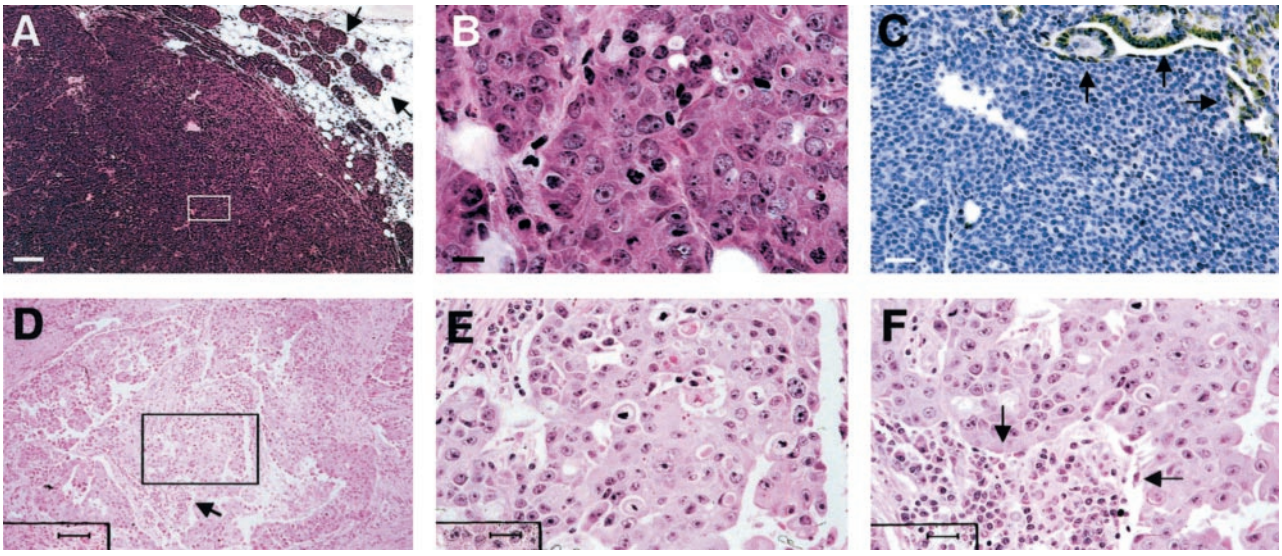

Figure 4. The late carcinoma in PyMT mice is comparable with human invasive ductal carcinoma. **A** and **B:** H&E staining of mammary sections from a PyMT mouse at 15 weeks of age. Note that tumor consists mainly of a solid sheet of cells. **Arrows** point to the areas adjacent to the primary tumor consisting of early-stage tumor acini. The **inset** in **A** is shown in **B**. **C:** IHC of laminin α1 in a tumor at late carcinoma stage. **Arrows** point to positively stained duct in the tumor. **D:** H&E staining of a human invasive carcinoma. The **inset** in **D** is shown in **E**. Note the pleomorphic nuclei in the section. The **arrow** in **D** points to a leukocytic infiltration site, which is shown in **F**. Scale bars: 100 μm (**A**, **D**); 10 μm (**B**); 25 μm (**C**, **E**, **F**). Original magnifications: ×100 (**A**, **D**); ×1000 (**B**); ×400 (**C**, **E**, **F**).

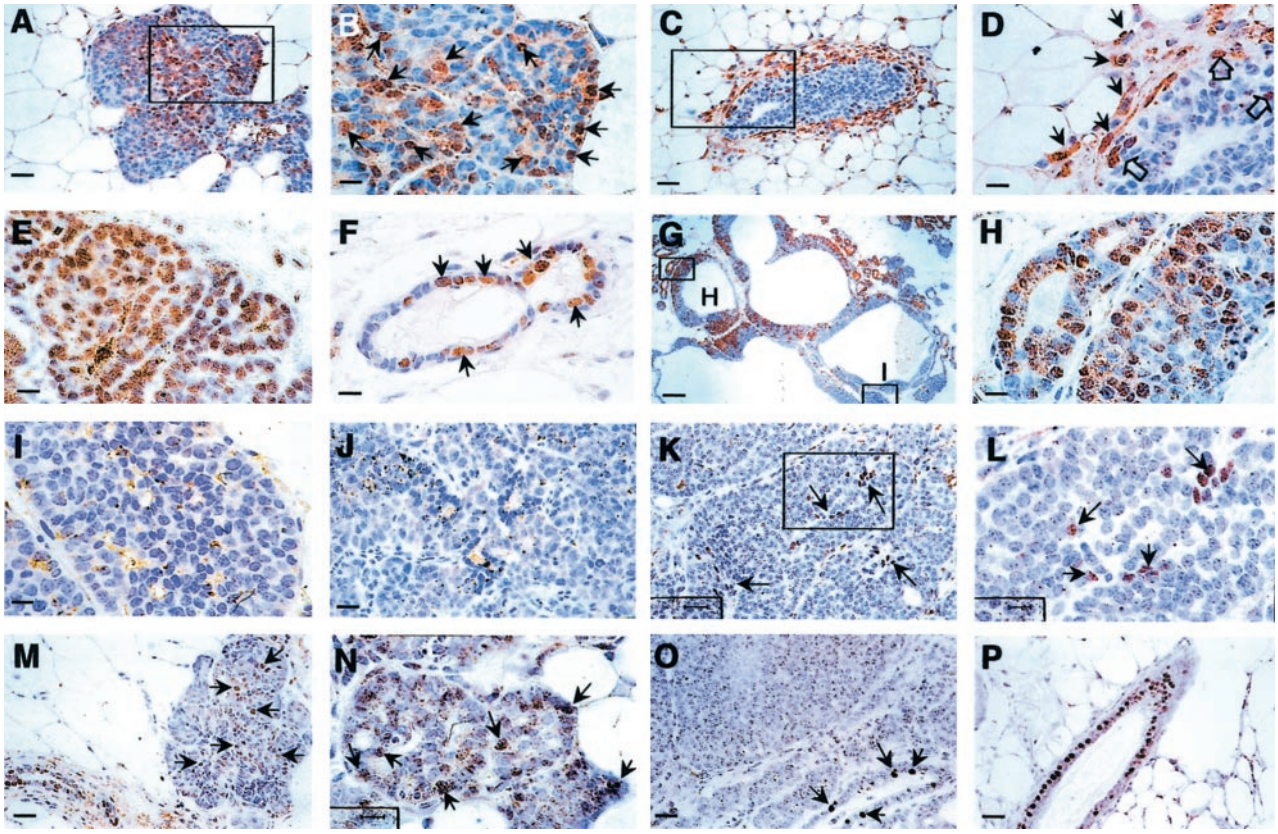

Figure 5. Loss of ER and PR during tumor progression to malignancy in the PyMT model. **A** to **L:** IHC of ER-α. Positive cells are stained in brown. **A:** Hyperplastic lesion from a PyMT mouse at 4 weeks of age. The **inset** in **A** is shown in **B**. **Arrows** point to some of the ER-positive cells. **C:** TEB adjacent of the hyperplastic lesion shown in **A**. The neck of the TEB (**inset**) is shown in **D** with higher magnification. **Arrows** point to ER-α-positive stromal cells and **open arrows** point to ER-α-positive epithelial cells in the TEB. **E:** ER-α staining of a primary mammary lesion at adenoma/MIN stage from a PyMT mouse at 8 weeks of age. **F:** A morphologically normal duct adjacent to the primary lesion shown in **E**. **Arrows** point to some of the ER-α-positive cells. **G** to **I:** Mosaic staining of ER-α in tumor at the early carcinoma stage. **G:** A tumor section from a PyMT mouse at 14 weeks of age. The **inset H** is in an area with high density of ER-α-positive cells and shown in **H**. **Inset I** is in an area with low-density staining and shown in **I**. **J:** A representative staining of ER-α in primary tumor at the late carcinoma stage (18 weeks of age). **K:** An area from the same tumor consisting of a limited number of ER-α-positive cells (**arrow**). The **inset** in **K** is shown in **L** with higher magnification. **Arrows** point to the positively stained cells. **M** to **P:** IHC of PR in mammary tumors from PyMT mice. **M:** A representative staining of PR in the hyperplastic lesion of a PyMT mouse at 6 weeks of age. **Arrows** point to some of the positively stained cells. **N:** Staining in an adenoma/MIN from a PyMT mouse at 8 weeks of age. **Arrows** point to some PR-positive cells. **O:** A representative PR staining of tumor at the late carcinoma stage. The tumor is from a PyMT mouse at 15 weeks of age and **arrows** point to PR-positive cells in a residual duct. **P:** Mammary section from a PyMT mouse at 8 weeks of age showing a representative staining of PR in morphologically normal mammary duct. Scale bars: 25 μm (**A**, **C**, **K**, **M**, **O**, **P**); 10 μm (**B**, **D**, **E**, **F**, **H**, **I**, **J**, **L**, **N**); 100 μm (**G**). Original magnifications: ×100 (**G**); ×1000 (**B**, **D**, **E**, **F**, **H**, **I**, **J**, **L**, **N**); ×400 (**A**, **C**, **K**, **M**, **O**, **P**).

chemistry (IHC). When the primary tumor in PyMT mice develops to hyperplasia stage, most of mammary glands with this stage of tumor (4 to 6 weeks of age) are at early pubertal development.[22] Primary tumors usually contain 30 to 40% of ER-α-positive nuclear stained cells (Figure 5, A and B, arrow). In normal ducts, the high density of ER-α-positive staining is not found in the epithelial cells but in stromal cells surrounding the terminal end buds (TEBs) (Figure 5, C and D, arrow) although some epithelial cells are positive (Figure 5D, open arrows). Many of these ER-α-positive stromal cells are mononuclear with elongated cell bodies and are distributed at the neck of the TEB, a site where a high density of macrophages is also found (Figure 5D).[19] In contrast to the TEB, fewer stromal cells are observed around the tumor acini at this stage (Figure 5, A and B) with the tumor often abutting directly on white adipose cells and these cells are ER-negative. This is similar to the structure surrounding the acini during pregnancy.[25] A marked increase of ER-α-positive cells is observed in the primary tumors that develop to the adenoma/MIN stage, with the density of the positive cells in the primary tumors varying from 50 to 80%. Half of the PyMT mice examined at this stage have ER-α-positive cells in tumor that reaches 80% of the total (Figure 5E). The variation of ER-α expression may be related to the stage of estrous cycle, as most of the PyMT mice carrying the adenoma/MIN-stage tumor are at the mid-pubertal developmental stage (7 to 8 weeks of age).[22] Most ducts in the mammary gland at this stage are morphologically normal and consist of ~50% ER-α-positive cells (Figure 5F, arrow) but some reach 80% positive as described.[26]

A marked change in the distribution of ER-α-positive cells is observed in some of the primary tumors as they develop to the initial malignant early carcinoma stage (8 to 12 weeks of age), (Figure 5G). The staining in the tumors appears mosaic with some areas containing a high density of ER-α-positive cells (Figure 5G, box H, and Figure 5H) while other areas are primarily negative [Figure 5G (box I) and I]. Interestingly, the population of

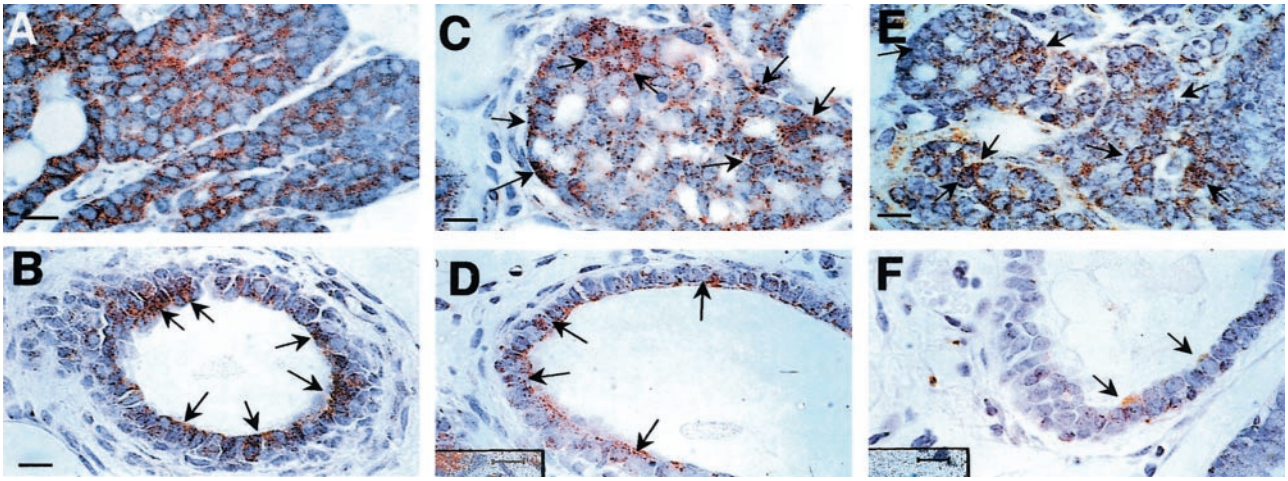

Figure 6. The expression of Neu increases during tumor progression to malignancy. IHC of Neu in mammary gland section of PyMT mice at various ages. **A:** A representative staining of Neu in a mammary gland carrying the primary lesion at the hyperplasia stage (4 to 5 weeks of age). **B:** An adjacent morphologically normal duct. **C:** Neu staining of a mammary gland with a primary lesion at the adenoma/MIN stage (6 weeks of age) and its duct (**D**). **E:** A representative staining of Neu in a mammary gland carrying a primary tumor at the late carcinoma stage (13 weeks of age) and its adjacent normal duct, **F**. **Arrows** point to some of the positively stained areas. Scale bars, 10 μm.

ER-α-negative cells appears to expand once the primary tumor progress to the late carcinoma stage (Figure 5, J and K). This phenomenon is observed in ~80% of PyMT mice carrying primary tumors at the late carcinoma stage. In these tumors, the ER-α-negative cells occupy more than 90% of the entire tumor section (Figure 5J) with only scattered clusters of ER-α-positive cells in limited areas (Figure 5, K and L, arrow). In the other 20% of PyMT mice with late carcinoma-stage tumors, the density of ER-α-positive cells in tumors remains ~40 to 50% suggesting that these tumors have still not progressed to the most malignant stage.

The onset of the expression of PR appears later than ER-α in the PyMT mammary gland. More than 80% of PyMT mice examined between 4 to 6 weeks of age have negative or low density (10 to 20%) of PR nuclear staining in the primary tumor (Figure 5M). The expression of PR in the ducts and TEB is observed after the onset of ovarian function (5 to 6 weeks of age) and the density of positive cells (40 to 60%) remains constant in these normal epithelial structures even when tumors in the same mammary glands have developed to malignant stages (Figure 5P). These data are consistent with previous reports of PR expression in normal mouse mammary glands and the responsiveness of PR gene expression to estrogen.[27] In contrast to the normal mammary ducts, when the primary tumors have developed to adenoma/MIN and early carcinoma stage (8 to 10 weeks of age) an increase of PR-positive cells (70 to 80% of total cells) is observed in ~30% of PyMT mice examined (Figure 5N). However, when the primary tumors have developed to the late carcinoma stage, in all of the mice examined, there are virtually no PR-positive cells in the tumor, except in the residual ductal structures inside or adjacent to the tumor [Figure 5, O (arrows) and P]. Therefore, similar to the expression of ER, the population of PR-positive cells is initially elevated followed by a marked decrease in the tumors that have developed to the malignant carcinoma stages.

Elevated Expression of ErbB2/Neu Is Found in the Late Carcinoma Stage

ErbB2/Neu expression has been found in human breast cancer patients with poor prognosis.[14] In the PyMT mouse, immunohistochemical staining for Neu with an antibody, that detects the cell surface and cytoplasmic forms of Neu, shows that it is expressed in all of the different stages of the primary tumor as well as in mammary ductal cells (Figure 6). However, the expression ratio of tumor and normal epithelium increases during the malignant transition of the tumor. At the hyperplasia stage, staining of the Neu protein is similar in the primary tumors and ducts (Figure 6, A and B, respectively) as well as in the TEB (data not shown). When the tumor has progressed to the adenoma/MIN stage, the intensity of the Neu staining in the primary tumor (Figure 6C) is much stronger than in the morphologically normal ducts in the same mammary gland (Figure 6D). This difference becomes more obvious when the tumors have developed to the carcinoma stage (Figure 6, E *versus* F), at which stage, most of the morphologically normal ducts have less than 50% positive cells and the intensity of the staining in these positive cells (Figure 6F) is much lower than the tumor (Figure 6E). The distribution of the Neu staining in malignant primary tumor is not even. The most intense staining is mainly observed in the center of the tumor.

These data suggest that ErbB2/Neu expression is initially high in the mammary epithelial cells of the TEB and the duct during early ductal development but is reduced once the development of the duct is complete. In contrast, elevated or persistent expression occurs as the

tumor advances, with especially high levels of expression seen in late carcinomas.

Redistribution of Cyclin D1-Expressing Cells Is Found during Tumor Progression

The expression of cyclin D1 is found in both the primary tumor and the developing mammary gland of PyMT mice. There is an increase in number and a redistribution of positive cells in the tumor as it develops to the carcinoma stage while at the same time the expression in normal ducts decreases. At the hyperplasia and adenoma/MIN stages, cyclin D1 positively stained cells (nuclear staining) are mainly located at the outer layer of the tumor acini (Figure 7B, arrows), which are located at the vicinity of the primary lesion (Figure 7A). The distribution of the positive cells in tumor acini appears similar to the distribution observed in normal TEBs in which cyclin D1-positive cells are also located at the outer layer of the structure (Figure 7C, arrows). At this age, more than 50% of epithelial cells in the developing ducts (Figure 7D) and ~40% in the TEB (Figure 7C) are positive for cyclin D1. This percentage is higher than observed in the primary tumor, which consists of 20 to 30% positive stained cells (Figure 7A).

In addition to an increase of cyclin D1-positive cells in the primary tumors that developed to the early carcinoma stage, the distribution of the positive cells in the lesion at this stage is different from tumors at the premalignant stages. Positive cells are now distributed through the entire tumor (Figure 7, E and F). At the most advanced stage of carcinoma, the highest density of cyclin D1-positive cells appeared in clusters within the tumor (Figure 7G). In these clusters, although the distribution of the positive cells is similar to the distribution observed in the tumor at the early carcinoma stage, the density of the positive cells is much higher (Figure 7, G and H).

Loss of Integrin-β1 in the PyMT-Induced Tumors

Studies have shown that integrin-β1 plays an important role in maintaining the orientation of the normal mammary epithelium and changes of its expression are associated with tumorigenesis in the breast.[28] We found that abnormal expression of this integrin occurs at an early stage of tumor development in PyMT mice. IHC using an anti-integrin-β1 antibody shows that, in developing mammary glands, the expression of integrin-β1 is found at the base of the epithelium in normal ducts (Figure 8; A to C, arrows). Light staining of integrin-β1 is found in hyperplastic lesions in the same mammary gland (Figure 8, A and B, open arrow). When tumors progressed to the late carcinoma stage, no integrin-β1 staining is found in center of the tumor (Figure 8D, open arrows), however, staining is still observed surrounding the residual ducts and early stage of hyperplasia in the distal areas of the same mammary gland (Figure 8E, arrows). Thus a loss of β1-integrins is strongly associated with tumor progression.

Marker Expression Detected by Immunoblotting Is Consistent to the IHC

To validate the IHC results, the same antibodies were also used to probe Western blots of protein lysates of age-matched mammary glands and tumors at different stages of progression that had been carefully dissected away from the surrounding tissues. Uterus and mammary gland from hormonally treated mice were used as positive controls. Consistent with the IHC, anti-Neu antibodies detected a 194-kd band in the tumor samples at all stages (Figure 9A, Neu, lanes 5 to 13). Compared to the level in adenoma/MIN stage (Figure 9A, lanes 5 to 7), a threefold to fivefold increase of the protein Neu level is observed in the malignant tumors (Figure 9A, lanes 8 to 13). On the other hand, in normal mammary glands (Figure 9A, lanes 1 to 4), the level of Neu protein in a developing gland (lane 2), which is comparable to tumor at adenoma/MIN stage (Figure 9A, lanes 5 to 7), is approximately fivefold to sevenfold higher than mature glands (Figure 9A, lanes 3 and 4) indicating that a decrease of Neu expression occurs when mammary gland development is complete. This decrease of Neu expression in mature mammary glands (Figure 9A, lanes 3 and 4) and the increased expression of the protein in carcinoma-stage tumors (Figure 9A, lanes 8 to 13) contributes to a marked difference between these two samples (10- to 12-fold). These results are therefore consistent with the IHC, which shows a persistent, elevated expression of ErbB2/Neu in the malignant tumors and a developmentally regulated expression of the protein in morphologically normal mammary ducts in PyMT mice.

Anti-cyclin D1 antibodies recognizes a 36-kd protein in primary mammary tumors that have developed to the early or late carcinoma stages (Figure 9A; cyclin D1, lanes 8 to 13). Consistent with the IHC, a much lower level of the protein is detected in tumors at the premalignant stage (Figure 9A, lanes 5 to 7) or normal mammary glands at various ages (Figure 9A, lanes 1 to 4), compared to tumor at the malignant stages (Figure 9A, lanes 8 to 13). In fact at this level of detection, cyclin D1 expression could barely be detected in the developing mammary gland and adenoma/MIN-stage tumor.

The anti-ER-α antibody detects a protein of 62 kd in the uterus and mammary gland of an estrogen and progesterone treated wild-type mice (Figure 9B; ER-α, lanes 1 and 2), developing mammary gland (Figure 9B, lanes 3 to 5), and tumor (Figure 9B, lanes 6 to 8) from PyMT mice. The expression is reduced in the primary tumors during their transition from adenoma/MIN (Figure 9B; ER-α, lane 6) to carcinoma (Figure 9B, lanes 7 and 8). On the other hand, the level of PR, detected by the anti-PR antibodies as a ~120-kd protein in the uterus (Figure 9B, lane 1) and mammary glands (Figure 9B, lanes 2 to 8) is relatively constantly expressed. However, it is reduced as tumors progress from early to late carcinoma (Figure 9B; PR, lane 7 compared to 8).

It is very difficult to find a reliable quantitative control for Western blots in the mammary gland and its tumors, other than the traditional β-tubulin and GAPDH as a pro-

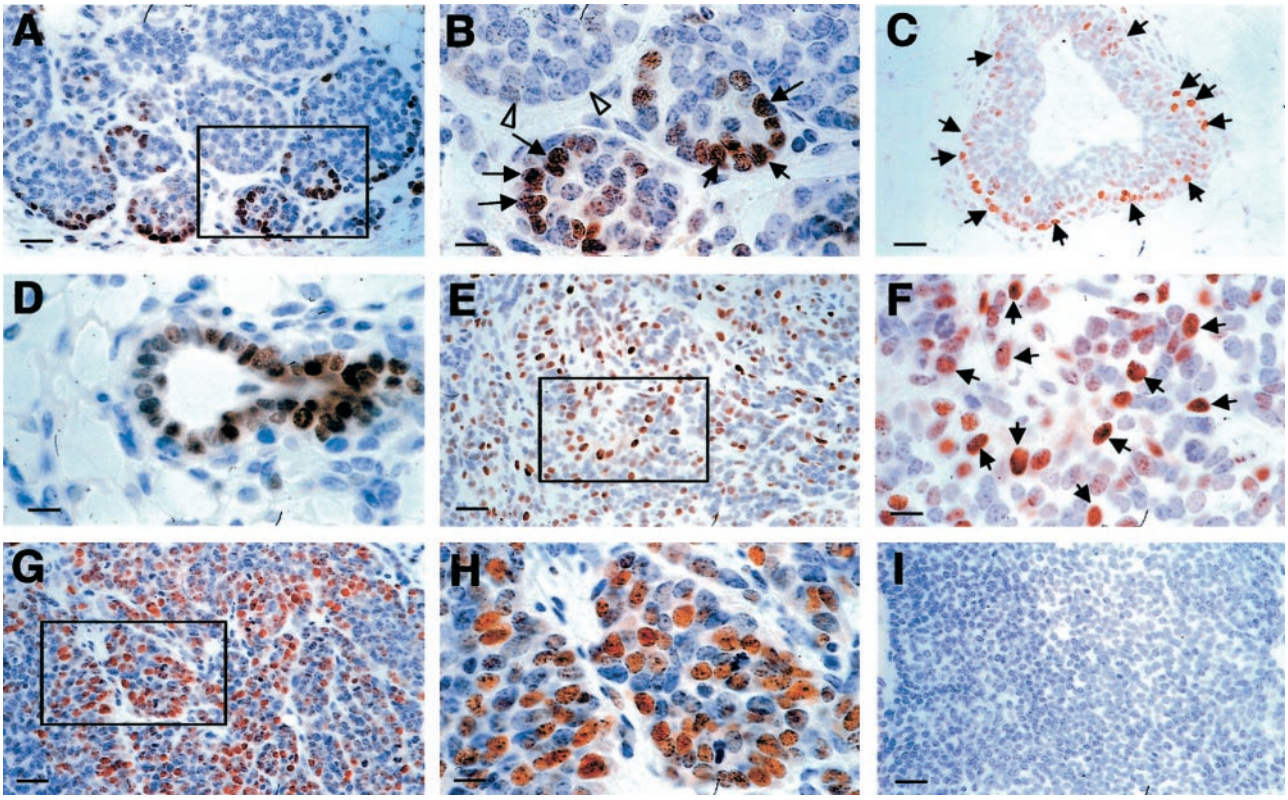

Figure 7. Increased expression of cyclin D1 during tumor progression to malignancy. **A** and **B:** Representative IHC of cyclin D1 in a PyMT-induced mouse mammary tumor at the adenoma/MIN stage (6 weeks of age). **A:** Positively stained cells are mainly found as a rim in the vicinity of the lesion. The **inset** in **A** is shown in **B**. **Arrows** point to cyclin D1-positive cells and **open arrows** point to adjacent acini that consist of mainly negatively stained cells. **C** and **D:** Cyclin D1 staining of an adjacent TEB and duct. **Arrows** point to positively stained cells. **E:** Cyclin D1 staining of a mammary tumor at the early carcinoma stage (9 weeks of age). The **inset** in **E** is shown in **F**. **Arrows** point to some of the positively stained cells. **G** and **H:** Staining of a primary tumor at the late carcinoma stage. The **inset** in **G** is shown in **H**. **I:** A mammary gland section stained with secondary antibody only as a negative control for the cyclin D1 IHC. Scale bars: 25 μm (**A**, **C**, **E**, **G**, **I**); 10 μm (**B**, **D**, **F**, **H**). Original magnifications: ×400 (**A**, **C**, **E**, **G**, **I**); ×1000 (**B**, **D**, **F**, **H**).

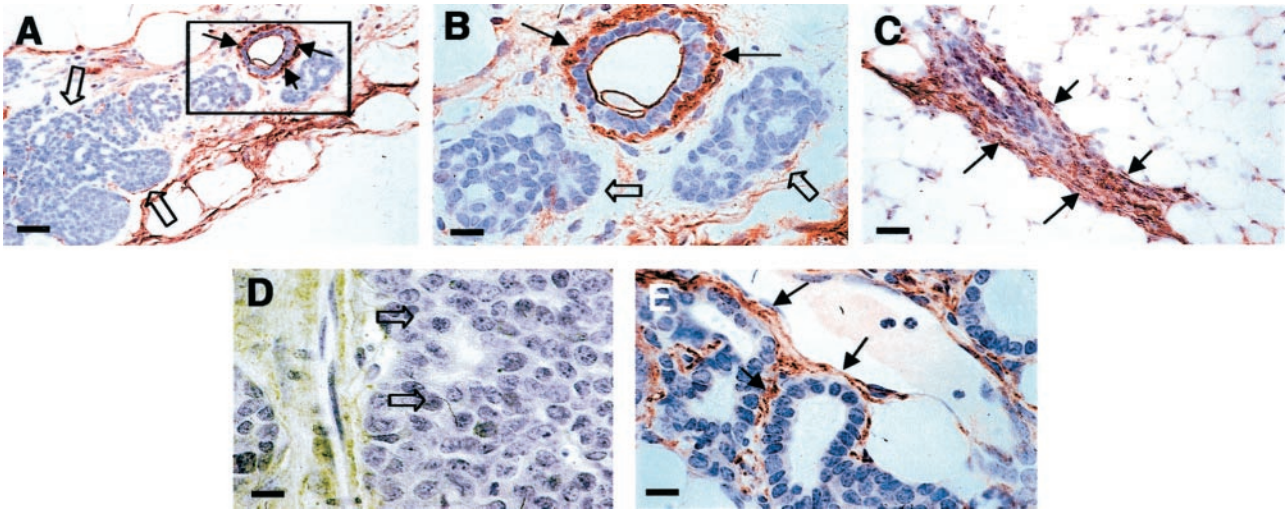

Figure 8. Lost expression of integrin-β1 in PyMT-induced lesions. **A** to **C:** IHC of integrin-β1 in mammary gland of a PyMT mouse at 4 weeks of age. **A:** Staining of primary lesion. Note that the positive staining is in the baseline of a morphologically normal duct (**arrows**) but no such staining is in the adjacent hyperplastic lesion (**open arrows**). The **inset** in **A** is shown in **B**. **Arrows** point to the positively stained areas and **open arrows** point to negatively stained adjacent hyperplastic lesions. **C:** The staining of a morphologically normal duct in the same mammary gland shown in **A**. **Arrows** point to positively stained areas. **D** and **E:** Staining for integrin-β1 of a PyMT-induced mammary tumor at late carcinoma stage. **D:** The primary tumor. **Arrows** point to the center of the tumor with negative staining of integrin-β1. **E:** Staining of secondary lesions in the same mammary gland. **Arrows** point to the positive stained area. Scale bars: 25 μm (**A, C**); 10 μm (**B**, **D**, **E**). Original magnifications: ×400 (**A**, **C**); ×1000 (**B**, **D**, **E**).

tein-loading control. This is because the tissue composition is constantly changing and, although keratin 8 is a good marker for epithelial content in the developing mammary gland, this keratin is lost in a random manner as the tumors progress. In addition, other keratins are expressed or lost in a sporadic manner (data not shown). Thus IHC may be more reliable method to determine the level of protein expression during tumor progression. Nevertheless, despite the high density of epithelial cells in the mammary tumor at the late carcinoma stage, both the ER-α and PR levels are lower in the tumor (Figure 9B, lane 8) compared to the normal mammary gland examined from 9 to 18 weeks (Figure 9B, lanes 3 to 5). This therefore, confirms the immunohistochemical data of loss of ER-α and PR expression as tumors progress.

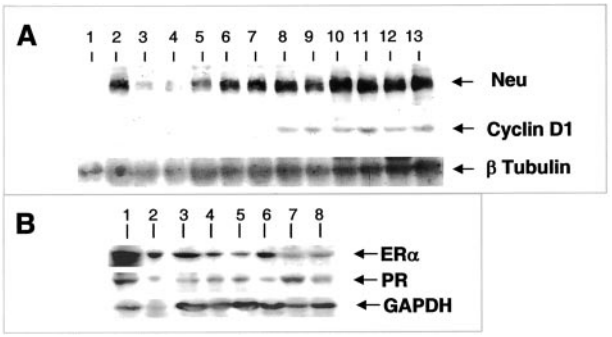

Figure 9. Western blot analysis of biomarker expression in mammary gland and tumor. **A:** Western blot analysis of Neu and cyclin D1 expression. **Lanes 1** to **4**, normal mammary glands from mice at 5, 9, 12, and 18 weeks of age, respectively. **Lanes 5** to **7**, mammary tumors at adenoma/MIN stage from three individual PyMT mice at 6, 6, and 10 weeks of age, respectively. **Lanes 8** to **10**, mammary tumors at early carcinoma stage isolated from three individual PyMT mice at 14 weeks of age. **Lanes 11** to **13**, mammary tumors at late carcinoma stage from PyMT mice at 18, 18, and 15 weeks of age, respectively. Ninety-six-kd Neu and 36-kd cyclin D1 bands are indicated. In this experiment, β-tubulin expression is used as the protein loading control. **B:** Western blot analysis of ER-α and PR in PyMT tumor and normal mammary glands. Uterus (**lane 1**) and mammary gland (**lane 2**) from an ovariectomized mouse treated with estrogen and progesterone for 2 days (16 weeks of age). **Lanes 3** to **5**, mammary glands from normal mice at 9, 12, and 18 weeks of age, respectively. **Lanes 6** to **8**, mammary tumors from PyMT mice at 10 (adenoma/MIN, **lane 6**), 14 (early carcinoma, **lane 7**), and 15 weeks of age (late carcinoma, **lane 8**).

Discussion

It is widely accepted that the tumorigenesis and progression of breast cancer constitute a multistep process that is influenced by many factors including genetic composition, age, hormonal status, and environment.[29] The multistep model of tumor progression suggests that invasive carcinoma derives from a series of intermediate hyperplastic and neoplastic stages.[2] The difficulties in managing the treatment of late stage or metastatic cancers has led to the goal for detection of early-stage disease.[2] In the attempt to identify early-stage mammary lesions that have the potential to develop to metastatic carcinoma, effort has been put into following up the development of clinically classified benign breast lesions.[30–32] These studies have identified certain proliferative breast lesions such as atypical hyperplasia and ductal carcinoma *in situ* with an increased risk to develop to malignant carcinoma. However, because of the limitation of clinical studies including the diversity of human genetic background and the difficulty in tumor and tissue procurement, our understanding of the biology of breast tumor progression, especially the connection between proliferative breast lesions and advanced carcinoma is still poor.

Many mouse mammary tumor models have been created in an attempt to reproduce the morphological and mechanistic characteristics of human breast cancer.[29] In an effort to mimic the human disease, rodent models with targeted gene mutations or deletions have been established based on the genetic alterations found in human breast tumors.[29] For instance, mice carrying inactivated BRCA1 and BRCA2 genes in the mammary epithelium, the common mutation found in women with a familial history of breast cancer,[33] developed mammary carcinoma that coincided with genome instability.[34] Numerous transgenic mice have been created to mimic the common chromosomal amplifications found in human breast cancer, such as c-*myc*, ErbB-2, and cyclin D1.[12,35] Although mammary carcinomas developed in these models, many of them appeared to have no or a low frequency of metastasis[36–40] suggesting that tumor progression to malignancy was not complete in these models. Furthermore, different from the observation in human studies that pregnancy reduced the risk of the breast cancer,[41] in some of the mouse models such as MMTV- or WAP-c-*myc* transgenic mice, multiple pregnancies required for tumor formation.[42]

The PyMT transgenic mice is one transgenic breast cancer model that exhibits a high frequency of pulmonary metastasis and the tumor formation in this model has a short latency and is pregnancy-independent.[7,8] Different from several other mouse models of breast cancer in which ductal hyperplasia occurs in the entire mammary epithelium,[21,43] a unique feature of tumor development in this model is that the primary mammary tumor, in most of the cases, develops as a single focus first on the ducts connected to the nipple.[7] It has been suggested that the PyMT oncoprotein subverts so many oncogenic pathways that it causes instantaneous transformation to the malignant state without the multiple steps required for most cancers. However, as the PyMT is expressed throughout the mammary epithelium the definition of four identifiable and sequential stages of tumor progression in the current study is not consistent with a single hit model but with a multihit phenomenon, with the PyMT acting as the initiating oncogene. Maglione and colleagues[44] who studied the early stages of progression in this PyMT tumor model arrived at a similar conclusion to ours. These workers derived transplantable hyperplastic lines from the premalignant tumors that retained their nonmalignant characteristics of the stage from which they were isolated even after prolonged periods of transplantation into syngeneic fat pads.[44] Thus it appears indisputable that the PyMT model also requires additional genetic events to progress to malignancy other than the expression of the PyMT oncogene events and as such provides a valuable model for the study of multistep progression to malignancy.

To stage these tumors precisely and to identify the events associated with the malignant switch is crucial for

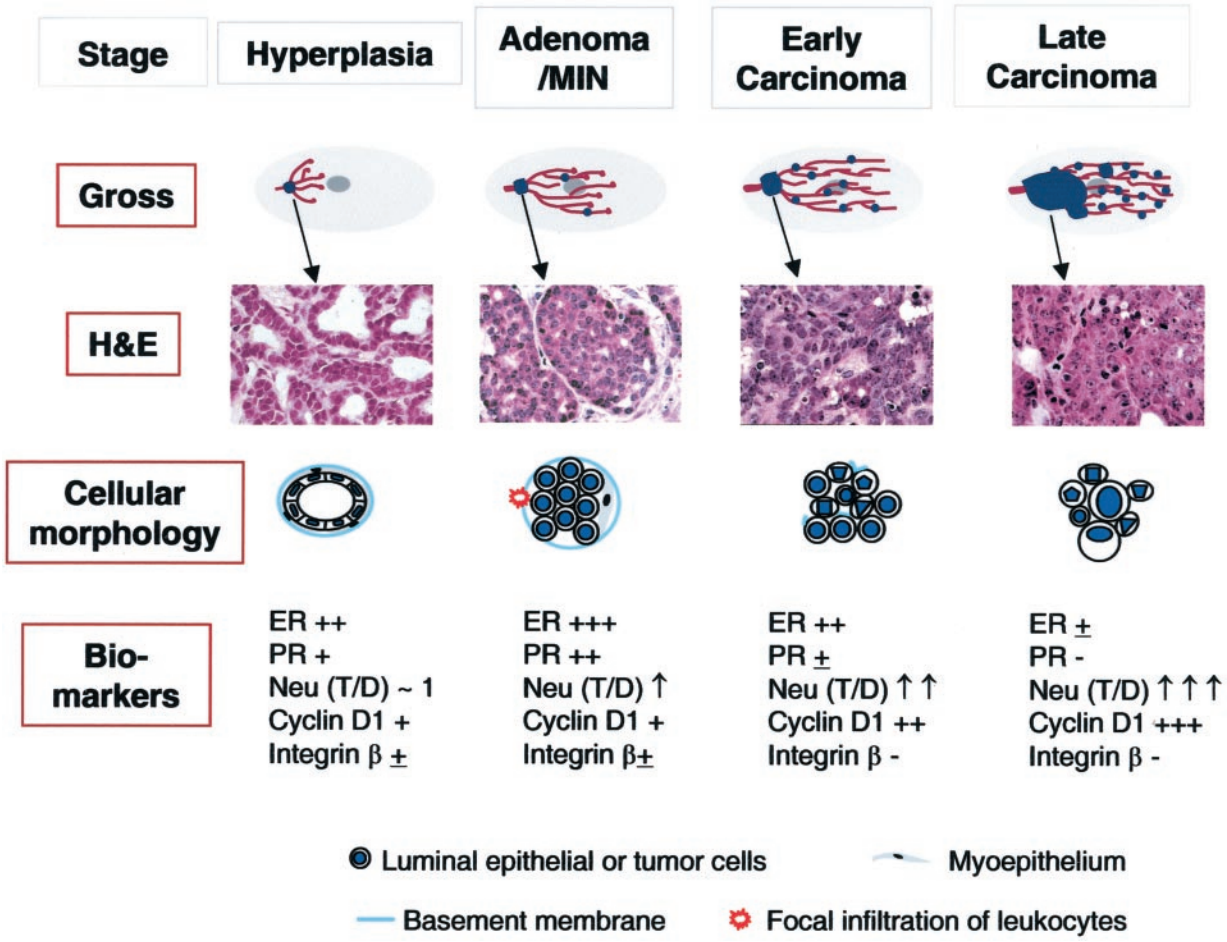

Figure 10. Summary of tumor progression and biomarker expression in PyMT mouse model of breast cancer. **Top**: Gross, displays the overall development of lesions in mammary glands of PyMT mice. Tumor lesions are indicated by **blue dots**. The H&E panel displays the corresponding histology of primary lesions at different stages of tumor progression. The cellular morphology panel schematically illustrates changes in the cytology of the cells as well as the integrity of the basement membrane and the presence or absence of myoepithelial and focal inflammation. Moreover, the changes in biomarkers during tumor progression is summarized in the panel of biomarkers. T/D, the ratio of Neu expression between lesions and normal ducts in age-matched mammary glands.

understanding the nature of the tumor progression and developing effective therapeutic strategies against cancer. For this purpose, we have developed a four-step classification of tumor progression and observed several similarities with human breast cancer progression. Maglione and colleagues[44] described a two-stage classification of PyMT tumors consisting of MIN and invasive carcinoma in the PyMT model. However, this does not easily allow focus on the early changes in proliferative lesions in PyMT model that may lead to the malignant switch. As summarized in Figure 10, this study has identified several such changes that are not only associated with altered cellular morphology in the tumor, but also with tumor growth, alteration of tumoral stroma, and host response to the tumor during the tumor progression to malignancy. Indeed, a number of these markers have been shown to be predictive of human breast cancer prognosis and perhaps to be causal in the disease process. Loss of estrogen and progesterone receptor gene expression has been found in 30% of human breast cancers, and this condition are associated with less differentiated tumors and poor clinical outcome.[13] Similarly, overexpression of ErbB2/Neu and cyclin D1 has been found in ~20% of cases and this also correlates with poor prognosis.[12,14] Remarkably, these phenomena seem to be recapitulated in the PyMT model with loss of ER and PR and overexpression of ErbB2/Neu and cyclin D1. This suggests a common pathway to malignancy between mammary cancers in mice and human. One difference in ER and PR expression between PyMT-induced tumor and human breast cancer is that a higher percentage of mice lost these receptors when the primary tumors developed to malignant stage (> 80% of mice *versus* ~30% human cases). This difference may reflect the relatively purer genetic background in mice compared to humans and this phenomenon can be useful in studying the mechanism of hormone resistance in human tumors.

By this detailed analysis of these early stages in tumor progression we have demonstrated a marked expansion of ER-negative cell population occurs in the tumor at the initial stage of the malignant transition. At this same early carcinoma stage, an increased expression of cyclin D1 and Neu as well as a redistribution of cyclin D1-positive cells in tumors, are also initiated. Together with the appearance of nuclear pleomorphism in the lesion, these data have demonstrated that a deregulation of cell pro-

liferation, which is the major feature of malignant transition, occurs in the stage defined here as early carcinoma (Figure 10).

Along with these intrinsic changes in the tumor cells that enhance their proliferative capacity and cause their loss of positional identity, we also observed consistent changes in the tumor stroma that were associated with this malignant transition from the adenoma/MIN to the early carcinoma stage. These changes include a loss of the integrity of the basement membrane and an incomplete surrounding by myoepithelium. Moreover, this study also identifies the loss of integrin-β1 expression in the earliest stage of the lesion, hyperplasia, in which the cellular morphology is still similar to the normal duct. Interestingly, the loss of basement membrane at the adenoma/MIN stage is focal and accompanied by a local increase of neovascularization, influx of inflammatory cells. Such leukocytic infiltration becomes significant in tumors developed to carcinoma stage and is often associated with tumor invasion suggesting that this early stromal change may in fact facilitate the development of tumor's ability to become invasive.

In this PyMT model we have already studied through genetic manipulation the role of the macrophage growth factor, CSF-1, whose overexpression was correlated with poor prognosis in human breast cancer.[45] These studies showed that CSF-1-regulated tumor-associated macrophages play an important role in the progression of PyMT tumors to metastasis and provided a casual exploration for the clinical data that correlated CSF-1 overexpression with poor prognosis.[7] Thus, we suggest that these inflammatory cells, and particularly the macrophages, provide trophic support to the tumor that includes the secretion of proteases to enhance basement membrane break down, the production of growth factors such as epidermal growth factor that stimulates cell motility and promotes cell viability as well as the synthesis of angiogenic factors. Therefore, at these sites of pronounced lymphocytic invasion, we propose that there would be a liberation of malignant cells from the tumor bed into the stroma where they are free to move to the newly formed vasculature and thus gain access to the circulation and consequently gain the ability to become metastatic. This model is consistent with the inhibition of metastasis in this PyMT model by the removal of macrophages.[7] It is also consistent with clinical data that shows the high frequency of tumor-associated macrophages with neo-angiogenesis and poor prognosis in human breast cancer.[46]

Taken together, this study demonstrates that our four-step method of classification of the PyMT model of breast cancer closely reflects the changes in tumors that progress from noninvasive to invasion. This classification system provides for the first time, precise information in identifying the malignant switch in the PyMT model and describing the features associated with this switch in the model. In addition, it is the first, in a transgenic model, to provide a comprehensive detailed histopathological and biological analysis of early proliferative lesions and to compare these with their counterparts of human disease. It emphasizes the proliferative shift and the loss of basement membrane integrity correlated with the influx of leukocytes at the malignant transition. This precise staging should allow causal events in tumor progression to be identified. It also suggests this model will be useful for preclinical therapeutic trials.

Acknowledgments

We thank James Lee and Leonid Gnatovskiy for excellent technical support, Hai Yan Pang for providing hormonally treated mice, and Dr. Y.-G. Yueng for providing antibodies against GAPDH.

References

1. Greenlee RT, Murray T, Bolden S, Wingo PA: Cancer statistics, 2000. CA Cancer J Clin 2000, 50:7–33
2. Lakhani SR: The transition from hyperplasia to invasive carcinoma of the breast. J Pathol 1999, 187:272–278
3. Merlino G: Regulatory imbalances in cell proliferation and cell death during oncogenesis in transgenic mice. Semin Cancer Biol 1994, 5:13–20
4. Green JE, Shibata MA, Yoshidome K, Liu ML, Jorcyk C, Anver MR, Wigginton J, Wiltrout R, Shibata E, Kaczmarczyk S, Wang W, Liu ZY, Calvo A, Couldrey C: The C3(1)/SV40 T-antigen transgenic mouse model of mammary cancer: ductal epithelial cell targeting with multistage progression to carcinoma. Oncogene 2000, 19:1020–1027
5. Furth PA: SV40 rodent tumour models as paradigms of human disease: transgenic mouse models. Dev Biol Stand 1998, 94:281–287
6. Macleod KF, Jacks T: Insights into cancer from transgenic mouse models. J Pathol 1999, 187:43–60
7. Lin EY, Nguyen AV, Russell RG, Pollard JW: Colony-stimulating factor 1 promotes progression of mammary tumors to malignancy. J Exp Med 2001, 193:727–740
8. Guy CT, Cardiff RD, Muller WJ: Induction of mammary tumors by expression of polyomovirus middle T oncogenes: a transgenic mouse model of a metastatic disease. Mol Cell Biol 1992, 12:954–961
9. Dankort DL, Muller WJ: Signal transduction in mammary tumorigenesis: a transgenic perspective. Oncogene 2000, 19:1038–1044
10. Asch BB: Tumor viruses and endogenous retrotransposons in mammary tumorigenesis. J Mammary Gland Biol Neoplasia 1996, 1:49–60
11. Dawe CJ, Freund R, Mandel G, Ballmer-Hofer K, Talmage DA, Benjamin TL: Variations in polyoma virus genotype in relation to tumor induction in mice. Characterization of wild type strains with widely differing tumor profiles. Am J Pathol 1987, 127:243–261
12. Brison O: Gene amplification and tumor progression. Biochim Biophys Acta 1993, 1155:25–41
13. Lapidus RG, Nass SJ, Davidson NE: The loss of estrogen and progesterone receptor gene expression in human breast cancer. J Mammary Gland Biol Neoplasia 1998, 3:85–94
14. Menard S, Tagliabue E, Campiglio M, Pupa SM: Role of HER2 gene overexpression in breast carcinoma. J Cell Physiol 2000, 182:150–162
15. Bieche I, Lidereau R: Genetic alterations in breast cancer. Genes Chromosom Cancer 1995, 14:227–251
16. Bissell MJ: The organizing principle: microenvironmental influences in the normal and malignant breast. Differentiation 2002, 70:537–546
17. Nguyen AV, Pollard JW: Colony stimulating factor-1 is required to recruit macrophages into the mammary gland to facilitate mammary ductal outgrowth. Dev Biol 2002, 247:11–25
18. Tong W, Pollard JW: Progesterone inhibits estrogen-induced cyclin D1 and cdk4 nuclear translocation, cyclin E, A-cdk2 kinase activation and cell proliferation in uterine epithelial cells in mice. Mol Cell Biol 1999, 19:2252–2264
19. Gouon-Evans V, Rothenberg ME, Pollard JW: Postnatal mammary gland development requires macrophages and eosinophils. Development 2000, 127:2269–2282
20. Sambrook J, Fritsch EF, Maniatis T: Molecular Cloning: A Laboratory

Manual. Cold Spring Harbor, Cold Spring Harbor Laboratory Press, 1989
21. Cardiff RD, Anver MR, Gusterson BA, Hennighausen L, Jensen RA, Merino MJ, Rehm S, Russo J, Tavassoli FA, Wakefield LM, Ward JM, Green JE: The mammary pathology of genetically engineered mice: the consensus report and recommendations from the Annapolis meeting. Oncogene 2000, 19:968–988
22. Richert MM, Schwertfeger KL, Ryder JW, Anderson SM: An atlas of mouse mammary gland development. J Mammary Gland Biol Neoplasia 2000, 5:227–241
23. Howard BA, Gusterson BA: Human breast development. J Mammary Gland Biol Neoplasia 2000, 5:119–137
24. Mallon E, Osin P, Nasiri N, Blain I, Howard B, Gusterson B: The basic pathology of human breast cancer. J Mammary Gland Biol Neoplasia 2000, 5:139–163
25. Gouon V, Lin EY, Pollard JW: Requirement of macrophages and eosinophils and their cytokines/chemokines for mammary gland development. Breast Cancer Res 2002, 4:155–164
26. Neville MC, McFadden TB, Forsyth I: Hormonal regulation of mammary differentiation and milk secretion. J Mammary Gland Biol Neoplasia 2002, 7:49–66
27. Shyamala G: Progesterone signaling and mammary gland morphogenesis. J Mammary Gland Biol Neoplasia 1999, 4:89–104
28. Roskelley CD, Bissell MJ: The dominance of the microenvironment in breast and ovarian cancer. Semin Cancer Biol 2002, 12:97–104
29. Blackshear PE: Genetically engineered rodent models of mammary gland carcinogenesis: an overview. Toxicol Pathol 2001, 29:105–116
30. Black MM, Barclay TH, Cutler SJ, Hankey BF, Asire AJ: Association of atypical characteristics of benign breast lesions with subsequent risk of breast cancer. Cancer 1972, 29:338–343
31. Dupont WD, Page DL: Risk factors for breast cancer in women with proliferative breast disease. N Engl J Med 1985, 312:146–151
32. Betsill Jr WL, Rosen PP, Lieberman PH, Robbins GF: Intraductal carcinoma. Long-term follow-up after treatment by biopsy alone. JAMA 1978, 239:1863–1867
33. Couch FJ, DeShano ML, Blackwood MA, Calzone K, Stopfer J, Campeau L, Ganguly A, Rebbeck T, Weber BL: BRCA1 mutations in women attending clinics that evaluate the risk of breast cancer. N Engl J Med 1997, 336:1409–1415
34. Xu X, Wagner K-U, Larson D, Weaver Z, Li C, Ried T, Henninghausen L, Wynshaw-Boris A, Deng C-X: Conditional mutation of Brca1 in mammary epithelial cells results in blunted ductal morphogenesis and tumour formation. Nat Genet 1999, 22:37–43
35. Buckley MF, Sweeney KJ, Hamilton JA, Sini RL, Manning DL, Nicholson RI, deFazio A, Watts CK, Musgrove EA, Sutherland RL: Expression and amplification of cyclin genes in human breast cancer. Oncogene 1993, 8:2127–2133
36. Matsui Y, Halter SA, Holt JT, Hogan BL, Coffey RJ: Development of mammary hyperplasia and neoplasia in MMTV-TGF alpha transgenic mice. Cell 1990, 61:1147–1155
37. Andres AC, Schonenberger CA, Groner B, Hennighausen L, LeMeur M, Gerlinger P: Ha-ras oncogene expression directed by a milk protein gene promoter: tissue specificity, hormonal regulation, and tumor induction in transgenic mice. Proc Natl Acad Sci USA 1987, 84:1299–1303
38. Sandgren EP, Schroeder JA, Qui TH, Palmiter RD, Brinster RL, Lee DC: Inhibition of mammary gland involution is associated with transforming growth factor alpha but not c-myc-induced tumorigenesis in transgenic mice. Cancer Res 1995, 55:3915–3927
39. Tsukamoto AS, Grosschedl R, Guzman RC, Parslow T, Varmus HE: Expression of the int-1 gene in transgenic mice is associated with mammary gland hyperplasia and adenocarcinomas in male and female mice. Cell 1988, 55:619–625
40. Maroulakou IG, Anver M, Garrett L, Green JE: Prostate and mammary adenocarcinoma in transgenic mice carrying a rat C3(1) simian virus 40 large tumor antigen fusion gene. Proc Natl Acad Sci USA 1994, 91:11236–11240
41. Russo IH, Russo J: Role of hormones in mammary cancer initiation and progression. J Mammary Gland Biol Neoplasia 1998, 3:49–61
42. Jamerson MH, Johnson MD, Dickson RB: Dual regulation of proliferation and apoptosis: c-myc in bitransgenic murine mammary tumor models. Oncogene 2000, 19:1065–1071
43. Li Y, Hively WP, Varmus HE: Use of MMTV-Wnt-1 transgenic mice for studying the genetic basis of breast cancer. Oncogene 2000, 19: 1002–1009
44. Maglione JE, Moghanaki D, Young LJ, Manner CK, Ellies LG, Joseph SO, Nicholson B, Cardiff RD, MacLeod CL: Transgenic polyoma middle-T mice model premalignant mammary disease. Cancer Res 2001, 61:8298–8305
45. Sapi E, Kacinski BM: The role of CSF-1 in normal and neoplastic breast physiology. Proc Soc Exp Biol Med 1999, 220:1–8
46. Leek RD, Harris AL: Tumor-associated macrophages in breast cancer. J Mammary Gland Biol Neoplasia 2002, 7:177–189